Cerebral Cortex, May 2020;30: 2789–2803

doi: 10.1093/cercor/bhz275
Advance Access Publication Date: 7 March 2020
Original Article

ORIGINAL ARTICLE

Auditory Processing Deficits Are Selectively Associated with Medial Temporal Lobe Mnemonic Function and White Matter Integrity in Aging Macaques

Daniel T. Gray[1,2], Lavanya Umapathy[3], Nicole M. De La Peña[1,2], Sara N. Burke[4], James R. Engle[1,2], Theodore P. Trouard[2,5] and Carol A. Barnes[1,2,6,*],

[1]Division of Neural System, Memory and Aging, [2]Evelyn F. McKnight Brain Institute, [3]Electrical and Computer Engineering, University of Arizona, Tucson, AZ 85721, USA, [4]Evelyn F. McKnight Brain Institute, University of Florida, Gainesville, FL 32611, USA, [5]Department of Biomedical Engineering and [6]Departments of Psychology, Neurology and Neuroscience, University of Arizona, Tucson, AZ 85721, USA

Address correspondence to Carol A. Barnes. Evelyn F. McKnight Brain Institute, University of Arizona, Life Science North, Room 355, Tucson, AZ 85724-5115, USA. Email: carol@nsma.arizona.edu

Abstract

Deficits in auditory function and cognition are hallmarks of normative aging. Recent evidence suggests that hearing-impaired individuals have greater risks of developing cognitive impairment and dementia compared to people with intact auditory function, although the neurobiological bases underlying these associations are poorly understood. Here, a colony of aging macaques completed a battery of behavioral tests designed to probe frontal and temporal lobe-dependent cognition. Auditory brainstem responses (ABRs) and visual evoked potentials were measured to assess auditory and visual system function. Structural and diffusion magnetic resonance imaging were then performed to evaluate the microstructural condition of multiple white matter tracts associated with cognition. Animals showing higher cognitive function had significantly better auditory processing capacities, and these associations were selectively observed with tasks that primarily depend on temporal lobe brain structures. Tractography analyses revealed that the fractional anisotropy (FA) of the fimbria-fornix and hippocampal commissure were associated with temporal lobe-dependent visual discrimination performance and auditory sensory function. Conversely, FA of frontal cortex-associated white matter was not associated with auditory processing. Visual sensory function was not associated with frontal or temporal lobe FA, nor with behavior. This study demonstrates significant and selective relationships between ABRs, white matter connectivity, and higher-order cognitive ability.

Key words: auditory brainstem response, diffusion MRI, fimbria-fornix, hippocampal commissure, presbycusis

Introduction

Age-related hearing loss, or presbycusis, is the third most common chronic medical condition in older adults, impacting nearly 80% of individuals over the age of 80 to some degree (Gopinath et al. 2009; Wattamwar et al. 2017). The clinical and societal implications of presbycusis extend well past the obvious difficulties in processing acoustic information, as late-life hearing loss has been suggested to be a contributing factor for depression, social isolation, and frailty at older ages (Mick et al. 2014; Panza et al. 2015; Jayakody et al. 2018). Additionally, large longitudinal studies have indicated that moderate to severe hearing impairment may be a risk factor

for developing dementia in older adults (Lin 2011; Deal et al. 2017). The clinical importance of understanding the robustness of and the neurobiological mechanisms contributing to the potential association between presbycusis and age-related cognitive decline is highlighted by recent observations that individuals equipped with cochlear implants may experience a partial restoration of cognitive function (Jayakody et al. 2017). From a basic research perspective, understanding covariations in sensory and cognitive function across the lifespan may provide valuable insights into fundamental principles, by which neuronal networks compensate for, and adapt to, functional alterations that arise across the aging brain.

Experiments using animal models to understand the aging brain have yielded invaluable data ranging from molecular to electrophysiological to behavioral levels of analysis. Macaque monkeys have been used for decades to study the neurobiological mechanisms underlying presbycusis and age-related cognitive decline, although these brain functions have been studied independently of one another. Similar to older humans, it is clear that aged nonhuman primates undergo declines in both sensory and cognitive functions (Moore et al. 2006; Juarez-Salinas et al. 2010; Hara et al. 2012; Engle et al. 2013; Ng et al. 2015; Gray and Recanzone 2017). Experiments designed to acquire functional and behavioral measures of sensory and cognitive function within the same set of monkeys do not currently exist, and are an important step toward understanding the brain processes underlying the apparent association between sensory deficits and age-related cognitive decline (Humes et al. 2013). Toward this goal, the present study combines a battery of behavioral tests designed to probe frontal and temporal lobe-dependent cognitive functions, auditory brainstem response (ABR) and visual evoked potential (VEP) electrophysiological recordings, and diffusion magnetic resonance imaging (dMRI) tractography analyses of white matter tracts associated with cognitive processing (Fig. 1A). The results presented here provide evidence for domain-specific associations between auditory and cognitive function alongside anatomical evidence that the structural integrity of medial temporal lobe white matter is associated with acoustic information processing in aging macaque monkeys.

Materials and Methods

Animal Subjects

Five aged (mean: 26 years; range 24.25–30.8 years) and 7 adult (mean: 11.42 years; range: 10–15 years) female bonnet macaque monkeys (*Macaca radiata*) participated in the present experiments. Note, however, that not every monkey participated in every component of the study (see Table 1). Behavioral, structural MRI, and diffusion tensor imaging data from this same cohort of animals have been reported previously (Burke et al. 2014; Gray et al. 2017; Comrie et al. 2018). Semiannual health evaluations were performed on each animal by the veterinary staff at the University of Arizona (Tucson, AZ), and no monkey displayed health concerns prior to or during the experimental timeline. All monkeys were pair-housed in a temperature- and humidity- controlled vivarium, and were maintained on a 12-h light–dark cycle with ad libitum access to food and water. For cognitive testing, all monkeys underwent behavioral shaping to allow transport from the home vivarium to the behavioral testing apparatus (described below) via a specialized nonhuman primate holding box (dimensions: 50.8× 31.1 × 40 cm). All experimental protocols described here were approved by the Institutional Animal Care and Use Committee at the University of Arizona and complied with guidelines set by the National Institutes of Health.

Cognitive Testing

Testing Apparatus and Stimuli

All cognitive assessments were executed in a modified Wisconsin General Testing Apparatus (WGTA; Harlow and Bromer 1938). The WGTA is composed of a holding compartment, in which the monkeys reside during behavioral testing. At one end of the box, vertical bars separate the animals from a panel containing three equally spaced circular holes that are used for stimulus presentation and food reward delivery. A wooden guillotine door that can be manipulated by the experimenter is used to control the monkeys' access to and visibility of stimuli. Additionally, the apparatus contains a transparent acrylic guillotine door to allow animals to view test objects without being able to interact with them. A one-way mirror separates the experimenters from the monkeys, allowing for the animals' performance to be overseen without detection. Stimuli include plastic toy objects of comparable size (~8 cm^3). Fresh fruit, vegetables, and sugar-free candy were used as rewards. All of the data from the cognitive battery described below have been published (Burke et al. 2014; Gray et al. 2017; Comrie et al. 2018), thus only brief descriptions of each paradigm are presented here.

Concurrent Object Reversal Learning Procedure

A complete protocol for the object reversal learning paradigm is as described in Burke et al. (2014); Gray et al. (2017); and Supplementary Figure S1A. Briefly, during the initial object discrimination learning phase of the task, the monkeys were presented with 40 object pairs per session, in which only one object in the pair was baited with a food reward. A given object pair was encountered only once in a daily session. Monkeys were allowed to displace only one object of each presented pair and were rewarded only if the correct choice was made. The baited object did not change between testing sessions. Once animals reached learning criterion (90% over 5 consecutive sessions) they progressed to the reversal learning component of the task. Here, the rewarded and unrewarded object in each pair was switched, and the monkeys were required to learn these new association contingencies to the same 90% criterion across 5 consecutive days. The effects of reversal learning were quantified using a state-space model of the binary trial response data (Smith et al. 2004; Gray et al. 2017). This analysis estimates a learning curve, from which an estimated learning trial can be derived. The "learning trial" is thus the metric of learning used in this study.

Visual-Pattern Discrimination

Visual-pattern discrimination abilities were assessed in a smaller subset of these monkeys ($n = 4$ adult and $n = 3$ aged) using a discrimination task with LEGO (Billund, Denmark; Supplementary Fig. S2A) stimuli. The full protocol for this task has previously been described in detail (Burke et al. 2011). LEGOS were used in order to systematically vary the degree of overlap between patterns to be discriminated. Overlap scores were computed by dividing the total number of LEGO nobs that were the same between the two patterns by the total number of nobs in the two patterns. Similarities of 60, 71, 86, and 92% were used. As with the object discrimination task described above,

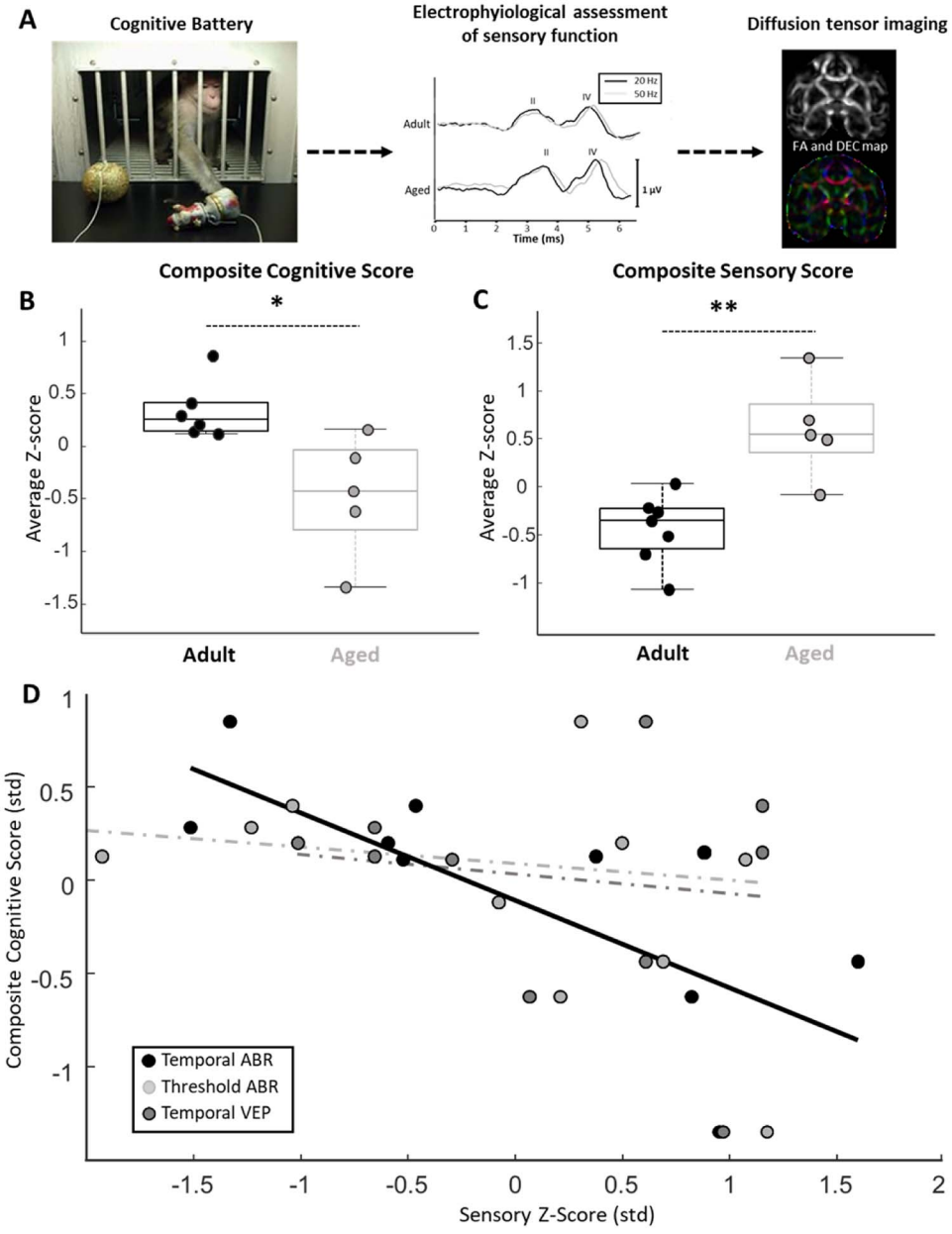

Figure 1. Schematic of experiment, composite cognitive and sensory scores, and the relationship between measures of sensory function and cognition. (*A*) Left panel: image of an aged bonnet macaque making a selection in the Wisconsin General Testing Apparatus used for the cognitive battery. Middle panel: representative temporal ABR recording from an adult and aged monkey. The black traces are derived from a recording, in which acoustic stimuli were presented at a rate of 20 Hz, whereas gray traces are derived from recording, in which the acoustic stimuli were presented at 50 Hz. Scale bar represents 1 µV. Right panel: FA and a directional encoded color (DEC) map obtained from diffusion-MRI analyses. (*B*) Box and whisker plot of composite cognitive scores for adult and aged macaques. Boxes denote the middle 50% of the data, and horizontal lines indicate the median of each distribution. Filled circles represent an individual monkey, with adult animals represented by black circles and aged animals with gray. Aged monkeys had lower composite cognitive scores relative to adults. (*C*) Box and whisker plot of composite sensory scores for adult and aged macaques. Box and whisker plot as in (*B*). Aged monkeys had higher composite sensory scores relative to adults. Note that greater values indicate poorer sensory function. (*D*) Scatter plot of z-score normalized measures of auditory processing (temporal ABR), auditory thresholds (threshold ABR), and visual system processing (temporal VEP) data plotted against composite cognitive scores. Solid trend line represents a significant relationship and dotted trend lines represent nonsignificant relationships. A significant relationship between auditory processing measures and composite cognitive scores was observed. * = $P < 0.05$; ** = $P < 0.01$.

one pattern was always associated with a reward, whereas the other was not. Monkeys performed 30 trials a day at each similarity level until reaching a performance criterion of 90% over 3 consecutive sessions. The number of errors performed before reaching criterion was the measure of visual-pattern discrimination learning used throughout this manuscript.

Reward Devaluation Procedure

The full protocol for the reward devaluation task (Supplementary Fig. S3A) is as described in detail in Burke et al. (2014) and Gray et al. (2017). Briefly, all animals underwent a food preference testing procedure to establish each individual monkey's food preferences. The monkeys were then trained on an object

Table 1 Table of monkey ages, the components of the study that each animal participated in (demarcated with an "X" in each respective column), and the reason for exclusion from a particular component of the project, if applicable

Monkey	Age (years)	Cognitive assessment	Sensory assessment	Diffusion MRI	Reason for exclusion
07 M06	25	X	X	X	
07 M05	24	X		X	Substantial noise in recording.
08 M01	32	X	X	X	
08 M02	24	X	X	X	
08 M03	11		X	X	Did not reach performance criterion
08 M04	11	X	X	X	
07 M04	26	X	X	X	
07 M08	15	X	X	X	
07 M11	14	X	X	X	
07 M12	14	X	X	X	
07 M10	14	X	X		Poor diffusion-MRI quality, tractography not possible
07 M09	14	X	X	X	

discrimination task, in which half of rewarded objects were always rewarded with a particular type of food while the other half were always rewarded with a distinct type of food, thus creating secondary associations between rewarded objects and food type. After the object discrimination phase, the monkeys completed the devaluation task. In these sessions, only the rewarded objects from the object discrimination training were used, and items were paired such that each choice would be reinforced with a distinct food reward. Monkeys were required to select only 1 of the 2 objects and retrieve the reward. Monkeys underwent baseline sessions where no food was given to animals before testing as well as selective satiation sessions, in which animals were given 1 of the 2 rewards ~10 min before testing. Each monkey also underwent the same testing procedure without objects, in which the reinforcement options were directly presented. This served to control for the possibility that the satiation procedures differentially modified food preferences in adult versus aged monkeys. The effect of reward devaluation was quantified using a difference score defined as the change in choices of each object/food type in selective satiation sessions relative to baseline sessions.

Delayed Nonmatching-to-Sample Procedure

Detailed descriptions of the delayed nonmatching-to-sample procedure used (Supplementary Fig. S4A) were as described in Comrie et al. (2018). Briefly, trials were initiated by the presentation of a single object over the center, baited well of the WGTA, and monkeys were allowed to displace the object and retrieve the food reward underneath it. The guillotine door was then lowered to impose a delay period of 10 s during training, and 15, 30, 60, 120, or 600 s during testing. Following the delay, the previously viewed sample object was presented alongside a novel one, and only the well underneath the novel object was baited. Monkeys learned through trial and error that the novel object was the baited object, and thus to make the correct response. All objects were unique across trials throughout the experiment. Training at the 10-s delay was carried out until animals reached a learning criterion of greater than 90% performance across 5 sessions. Five days of testing were completed at the remaining delays in sequentially increasing order. Acquisition data presented here are the number of completed trials required to reach the 90% learning criterion, and performance measures are the averaged proportion of correct responses across the 5 test delay conditions.

Delayed-Response Procedure

The delayed-response task (Supplementary Fig. S5A) used to assess visuospatial short-term memory is as described in detail by Comrie et al. (2018). Briefly, trials were initiated by raising the wooden guillotine door and dropping the acrylic glass door of the WGTA to allow monkeys to observe the experimenter bait one of the two lateral wells with food reward. Two identical opaque plaques were then used to cover the two lateral wells before dropping the guillotine door to obstruct the animal's view of the objects and impose a delay period of either 0, 1, 5, 10, 15, 30 or 60 s. Following the delay, both doors were lifted and the animals were allowed to displace just one of the plaques. If the monkey selected the baited plaque, then it was allowed to retrieve the food reward. The 0 and then 1 s delays were used during the training phase of the task. In both cases, a learning criterion of greater than 90% performance over 3 consecutive 30-trial sessions was used. Once criterion had been met, testing on the remaining delays was administered in sequentially increasing order. Acquisition data presented here are the number of completed trials required to reach the 90% learning criterion at the 1 s delay, and performance measures are the averaged proportion of correct responses across the 5 test delay conditions.

Composite Cognitive Score

Data from the tasks described above were z-score normalized in order to standardize the units of all data across tasks. In all cases the data were normalized so that higher z-score values indicate better performance on the tasks. All z-scores were averaged for every individual animal, and these values served as the composite cognitive score.

Assessment of Sensory Function

Auditory Brainstem and Middle Latency Responses

The auditory brainstem response (ABR; Supplementary Figs S6A,B,D) recording protocols followed guidelines published in previous nonhuman primate studies (Fowler et al. 2010; Engle et al. 2013; Ng et al. 2015). Monkeys were anesthetized with a mixture of ketamine (1.5–2.0 mg/kg) and DexMedetomidine (0.007–0.01 mg/kg) and placed in the prone position with their heads elevated. Soft insert earphones (etymotic ER3A transducers) were placed into each ear canal. The skin behind both ears, forehead, and back of the neck were sterilized with

an alcohol scrub, and 22-guage stainless steel electrodes were placed subcutaneously at each location (Allen and Starr 1978; Fowler et al. 2010). An Intelligent Hearing System (Smart EP Win USB, v. 3.97) on a laptop computer was used to acquire all evoked potentials. Stimuli consisted of 2, 8, 16, or 32 kHz pure-tone bursts, all delivered in a 10 ms trapezoidal envelope with a 2 ms rise/fall time. All acoustic stimuli were repeated a minimum of 2000 times to obtain reliable average evoked responses. Evoked signals were amplified by 100 000 and bandpass filtered between 100 and 1500 Hz to extract the ABR waveform. Peaks II and IV of the ABR were most reliably observed in these data, as has been reported previously in macaque recordings (Ng et al. 2015). Thus, only these two peaks were considered for this analysis. The latency of each peak was defined as the time from stimulus onset to the apex of the wave in consideration. In cases where no waveform was present at a given sound pressure level, no latencies were extracted. Latency data presented throughout this report consider only conditions, in which stimuli were presented at a sound pressure level of 60 dB. Peak amplitudes were not considered for these analyses as age-associated changes in bone density (Kiebzak 1991; Mosekilde 2000) can affect ERP amplitudes, possibly introducing an additional covariate that could lead create false-positives when interpreting these data. The frequency of presentation and intensity of auditory stimuli differed between the temporal and threshold ABR as described below.

Threshold ABR

All stimuli were presented binaurally at 50 Hz. Initially, all stimuli were presented at 80 dB peak sound pressure level. The intensity of the acoustic stimuli was then reduced in 20 dB steps until a discernable ABR waveform was no longer evident. Once the evoked response had disappeared, the sound intensity was raised by increments of 5 dB until the waveform was reestablished. The ABR threshold was taken as the average sound pressure level, at which the waveform was absent and the level where it was visible for the final time. See Supplementary Fig. S6A,B, for example threshold ABR recordings.

Temporal ABR

All acoustic stimuli were presented binaurally at 60 dB peak sound pressure level. Stimuli were first presented at 50 Hz, and then again at 20 Hz. Wave II and Wave IV peak latencies were calculated for the 20 and 50 Hz conditions, respectively, and the difference between the two (50 Hz minus 20 Hz) was used as the estimate of temporal auditory processing.

The temporal ABR was designed specifically to test temporal auditory processing deficits since threshold ABR measures are not sensitive to these impairments as they generally arise at suprathreshold sound intensity levels. Latency differences between conditions with different stimulus presentation rates are thought to reflect temporal auditory processing since it has been shown that ABR waveform latencies increase as the interval between acoustic stimuli decreases in forward masking paradigms (Mehraei et al. 2016). This shift is thought to reflect a reduced reliability of neural responses to faster stimuli, potentially due to a depletion of readily releasable vesicle pools (Mehraei et al. 2017). Importantly, latency differences between fast and slow interstimulus interval conditions correlate with perceptual gap detection capabilities, which is a psychometric test of temporal processing in the auditory system (Eggermont 2015; Mehraei et al. 2016; Mehraei et al. 2017). See Supplementary Fig. S6D, for example temporal ABR recordings.

Visual Evoked Potential

VEPs (Supplementary Fig. S6G) were acquired using the same Intelligent Hearing System (Smart EP Win USB, v. 3.97) software used to acquire the ABR recordings. Electrode placements followed the guidelines set by the manufacturer (Smart EP), with minor adjustments to translate the configuration from a human head to that of a macaque. Specifically, a midoccipital scalp electrode was placed roughly an inch above the inion. Right- and left-occipital electrodes were placed an inch to either side of the midoccipital location. A reference electrode was placed on the top of the scalp along the midline, and the ground was placed just posterior to the brow ridge. Animals were placed in the prone position with their heads elevated and looking forward. A full-field checkerboard pattern delivered via an Intelligent Hearing System VEP stimulator was used as the stimulus. The VEP stimulator was placed roughly 50 cm in front of the monkey's face. Stimuli were delivered at either 1 Hz or 2 Hz. All visual stimuli were repeated a minimum of 100 times to obtain reliable average evoked responses. Evoked signals were amplified by 100 000 and bandpass filtered between 1–300 Hz. The most reliably observed evoked potential in both adult and aged monkeys was a positivity around 75 ms, which will be herein referred to as P_{75} (Supplementary Fig. S6G). In some instances a second positivity was observed around 100 ms, but P_{75} was the only VEP signal analyzed for the present study since it was observed in every subject. The latency of each peak was defined as the time from stimulus onset to the apex of P_{75}. Latency data presented in this study were derived from the 1 Hz stimulus presentation conditions. Latency difference data were calculated by subtracting the P_{75} latency from 1 Hz stimulus presentation rate conditions from the 2 Hz condition to give an estimate of temporal processing in the visual system.

Composite Sensory Scores

Data from the threshold ABR, temporal ABR, and VEP were z-score normalized in order to standardize the units of all data. All z-scores were averaged for every individual animal and these values served as the composite sensory score. Note that for this measure, higher values reflect poorer function.

Diffusion Tensor Imaging and Tractography Protocol

Image Acquisition and preprocessing Protocol

In-depth descriptions of the image acquisition and preprocessing protocols are as in (Gray et al. 2018). Briefly, all MR images were acquired on a 3 T GE (General Electric, Milwaukee, WI) Signa scanner using a body coil for the radio frequency excitation and an 8-channel head coil for reception. Three scans were obtained for each monkey. 1) High-resolution anatomical whole-brain T1-weighted images were acquired with a 3D inversion-recovery prepped spoiled gradient-echo sequence, 2) T2-weighted reference scans using a fast spin-echo sequence, and 3) diffusion-weighted images using single shot echo planar imaging. Diffusion-weighted images were acquired over 51 diffusion directions in a HARDI sampling scheme over a single shell with a *b*-value of 1000 s/mm^2. Images were resectioned from the 3D volumes into coronal, sagittal and axial slices.

DICOM images were converted to NIFTI format and T1, T2, and dMRI images were skull stripped using manually drawn masks in MRIcron (https://www.nitrc.org/projects/

mricron). Eddy current distortions in DW images were corrected using an iterative Gaussian Process-based registration in the FMRIB Software Library (FSL) (Rasmussen and Williams 2006; Andersson and Sotiropoulos 2015). Distortions due to B0-field inhomogeneity were corrected using the TORTOISE software (Pierpaoli et al. 2010) by nonlinearly registering the DW images to reference T2 images. Coil inhomogeneity was corrected using N4ITK bias correction software (Tustison and Gee 2009; Tustison et al. 2010) and noise in DW images was removed using a local principal component-based noise removal algorithm described in (Manjón et al. 2013). DW images were registered to T1 images using FSL's Automated Segmentation Toolbox, followed by FSL's Linear Image Registration Tool and a Boundary-Based Registration algorithm (Greve and Fischl 2009). Fractional Anisotropy (FA) maps were generated from diffusion tensor fitting of the DW images in each subject's native space.

Tractography

Probabilistic streamlines were generated between regions of interest (ROI) masks in each subject's native space. Streamlines were generated using a multitensor tractography approach in FSL's Diffusion Toolbox, ProbtrackX, as described in detail in (Gray et al. 2018). This analysis output a probability map in each subject's diffusion space, in which the value of each voxel is the weighted probability that the voxel belongs to the anatomical pathway in question. To account for the possibility of partial volume effects impacting the FA estimates, T1-weigted images were segmented into gray matter, white matter, and CSF using FSL's Automated Segmentation Toolbox (FAST). This analysis outputs the probability that a given voxel belongs to each class of tissue. A value of 0.3 was used to threshold and binarize both the white matter and CSF maps. In the more conservative approach, the binarized white-matter mask was used to extract voxels in the probabilistic streamlines. These masked probability maps were then used to extract and average the FA along each pathway only in white matter. A second approach used the binary CSF mask to exclude voxels considered by the segmentation algorithm to be CSF, and the FA along each pathway was extracted using the remaining voxels (i.e., white matter and gray matter). In both approaches, FA values were normalized by summing the probability-weighted FA values by the sum of the total probability in the map. The FA values derived from each methods of correcting for partial volume were associated with cognitive and sensory function in qualitatively similar ways (compare Figs 3 and 4 and Supplementary Figs S7 and S8).

The advantage of using probabilistic tractography instead of ROI-based approaches in the macaque is 2-fold. First, tract-tracing anatomical studies in nonhuman primates have made it clear that fibers connecting two given regions are not uniformly distributed within the white-matter bundles, through which they course (Lehman et al. 2011). The voxel-by-voxel probabilistic weighting of the FA data is able to account for this heterogeneity, whereas ROI-based approaches that use predefined volumes instead of probabilistic streamlines cannot. Second, white-matter atlases are not readily available in macaques as they are in humans, but structural MRI atlases are (Bakker et al. 2015), thereby making it easier to standardize seed regions between studies.

Regions of Interest

All ROI masks were drawn on the T1 images using MRIcron software with guidance from the (Bakker et al. 2015) open source scalable macaque brain atlas. This atlas is based on 0.075 mm MRIs averaged over 10 macaque monkeys of comparable weight to the animals used in this study. ROIs for each extracted fiber tract will be described in turn below.

Thalamic Segmentation

Each thalamus was segmented using anatomical landmarks to yield ROIs contained within the anterior and mediodorsal thalamic nuclei. Importantly, these ROIs do not encompass the entirety of each thalamic region since the resolution of the scans was not sufficient to reliably demarcate the boundaries of each nucleus. Instead, this landmark-based approach is meant to provide conservative estimates of each nuclei's location with good intersubject consistency. The landmarks used to delineate each thalamic region are described below.

Anterior Thalamic Nuclei

The anterior border was set as the first section posterior to the anterior commissure to contain thalamic tissue. The posterior boundary was defined as the second section moving posteriorly in the coronal plane, after which the anterior aspect of the third ventricle splits into dorsal and ventral segments. Medially, the anterior nuclei ROI was bounded by the midline, and the lateral boundary was set by the internal medullary lamina.

Mediodorsal Thalamic Nuclei

The anterior boundary was set as the first section posterior to the most caudal extent of the anterior thalamic nuclei ROI. The posterior border was defined as the first coronal section anterior to the section, in which the dorsal aspect of the third ventricle rejoins the ventral aspect of the third ventricle. Medially, the mediodorsal nuclei ROI were bounded by the midline, and the lateral boundary was set by the internal medullary lamina.

Forebrain ROIs and Tractograhy Analyses

The procedures for drawing forebrain ROIs and the tractography analyses performed with each are discussed in turn. Right and left hemisphere pathways were tracked independently when applicable.

Frontal Cortex, Frontal Thalamic Radiation, and Anterior Commissure

The frontal pole was the anterior border of the frontal cortex ROI, and the posterior border was defined as the last section anterior to the genu of the corpus callosum. Streamlines were generated between the mediodorsal thalamic nuclei ROI and frontal cortex ROIs. An inclusion mask was drawn to encompass the white matter of the anterior segment of the internal, external and extreme capsules, roughly at the level of the temporal–frontal junction. Exclusion masks were used to prevent streamlines from entering the uncinate fasciculus and amagdalofugal pathways into the anterior temporal lobes, as well as along the longitudinal fasciculi to prevent streamlines from being generated posteriorly. To extract the anterior commissure, an inclusion mask was drawn through the midline of the anterior commissure, and exclusion masks were drawn to exclude posterior tracts, through the midline of the genu to exclude tracts through the corpus callosum, and through the midline of the brain beginning just anterior to the anterior commissure.

Hippocampus, Fimbria-Fornix, and Hippocampal Commissure

The entire anterior–posterior axis of the hippocampus was included in this ROI. The anterior border of this ROI was the

first section, in which the lateral ventricle at the junction of the posterior extent of the amagdaloid complex and the anterior hippocampus became visible. The posterior border was defined as the first section, in which the posterior extent of the lateral ventricles clearly gives way to hippocampal tissue, generally occurring around the level of the splenium. The medial boundary used was the border between the prosubiculum and the surrounding parahippocampal or entorhinal cortex (depending on A-P location), which occurs at the medial most apex of the medial temporal lobe. All subfields of the hippocampus proper were included in this ROI, as were the prosubiculum, subiculum, presubiculum, and parasubiculum. Streamlines were generated between the anterior thalamic nuclei ROI to the hippocampus ROI. Two inclusion masks were set: one at the dorsal-most extent of the fornix, just ventral to the corpus callosum and dorsal to the mediodorsal thalamic nuclei, and a second one posterior to the thalamus where the caudal fornix becomes the fimbria of the hippocampus, roughly at the level of the splenium. Exclusion ROIs were placed just anterior to the thalamus to prevent streamlines from being generated into the frontal and anterior temporal lobes via the frontal and inferior thalamic radiations and uncinate fasciculus. To extract the hippocampal commissure, streamlines were generated between the right and left hippocampi to traverse through the hippocampal commissure. An inclusion mask was drawn through the hippocampal commissure in the coronal sections, and exclusion masks were drawn to exclude fornix streamlines.

Statistical Analyses

Behavioral Assessment

The reversal learning, reward devaluation, and visual-pattern discrimination tasks were analyzed using repeated measures ANOVAs. Post hoc tests were performed in every case using unpaired *t*-tests. Delayed nonmatching-to-sample and spatial delayed-response trials to criterion and average performance across delays measures were analyzed with unpaired *t*-tests. In all cases an alpha level of 0.05 was used, and *P* values underwent Bonferroni–Holm correction when applicable.

Assessment of Sensory Function

ABR thresholds, latencies, and latency differences across different stimulus frequencies were analyzed with repeated measures ANOVAs. Analyses of ABR data averaged across stimulus frequencies, as well as MLR and VEP data were analyzed with unpaired *t*-tests. In all cases an alpha level of 0.05 was used, and *P* values were Bonferroni–Holm corrected when necessary.

FA Comparisons

FA estimates from each thalamocortical projection were analyzed using repeated measures ANOVAs with age group (adult and aged) and hemisphere (right and left) as factors. Post hoc tests were performed in every case using unpaired *t*-tests. Again, an alpha level of 0.05 was used.

Regression Analyses

The relationships between auditory, visual, and cognitive function, as well as the relationships between FA indices and sensory and/or cognitive function were assessed using a robust regression model. This regression method is an alternative to least-squares regression, and is commonly used with comparatively smaller datasets since it is more robust in the presence of outliers. In the auditory to cognitive function correlations, auditory scores were the independent variables and cognitive scores the dependent variables. In the FA to cognitive/sensory function correlations, FA was the independent variable and cognitive/sensory scores the dependent variables. In all cases the significance criterion was $P < 0.05$.

Results

Auditory Temporal Processing Is Associated with Cognitive Performance

Adult and aged monkeys completed a battery of six distinct behavioral tests designed to probe frontal and temporal lobe-dependent cognitive functions. Composite cognitive scores indicated that older monkeys were significantly worse (lower *z*-score) than were adults in performing the battery (*t*-test; $n_{adult} = 6$, $n_{aged} = 5$; $P = 0.013$, $t = 3.06$; Fig. 1*B*). Importantly, the aged macaques were only impaired on tests of concurrent reversal learning, visual discrimination, and reward devaluation; whereas adult and aged animals performed equivalently on tests of object discrimination, object recognition memory, and spatial short-term memory (see Supplementary Figs S1–S5). This selectivity indicates that age-related declines in distinct aspects of cognition arise partially independently of one another in macaques as is the case in humans (Glisky et al. 1995; Fernandes et al. 2004). The same monkeys also underwent three distinct tests of auditory and visual system function using electrophysiological techniques. Composite sensory scores indicated that sensory functioning was also significantly worse (higher *z*-score) in the older animals compared to the adults (*t*-test; $n_{adult} = 7$, $n_{aged} = 5$; $P = 0.0019$, $t = -4.16$; Fig. 1*C*). Again, despite clear age differences in this composite sensory score, the older animals were not impaired on all measures. In particular, adult and aged monkeys did not differ in their auditory thresholds or visual system function, whereas older animals showed clear auditory processing deficits as assessed by the temporal ABR (see Supplementary Fig. S6).

Relationships between the three measures of sensory function and the composite cognitive scores were assessed. This analysis revealed that animals with less efficient auditory processing abilities had lower overall cognitive scores than did animals with better auditory processing capacities (robust regression; $n = 10$; $P = 0.027$, $r = -0.72$, $t = -2.70$; Supplementary Fig. 1*D*). On the other hand, auditory thresholds and visual system function were not related to the composite cognitive scores (robust regression, ABR threshold: $P = 0.61$, $r = -0.39$, $t = -0.52$; temporal VEP, $P = 0.72$, $r = -0.20$, $t = -0.38$; Fig. 1*D*).

Task-Specific Relationships between Auditory Processing and Cognition

Next, relationships between the measures of auditory processing and performance on each individual behavioral task were assessed to determine which specific cognitive operations were associated with hearing function. This analysis revealed that only certain cognitive functions were related to auditory processing, whereas others were not. In particular, better auditory processing was significantly associated with better performance on the tests of concurrent reversal learning (robust regression; $n = 10$; $P = 0.037$, $r = 0.67$, $t = 2.50$; Fig. 2*A*), object recognition memory (robust regression; $n = 10$; $P = 0.00056$,

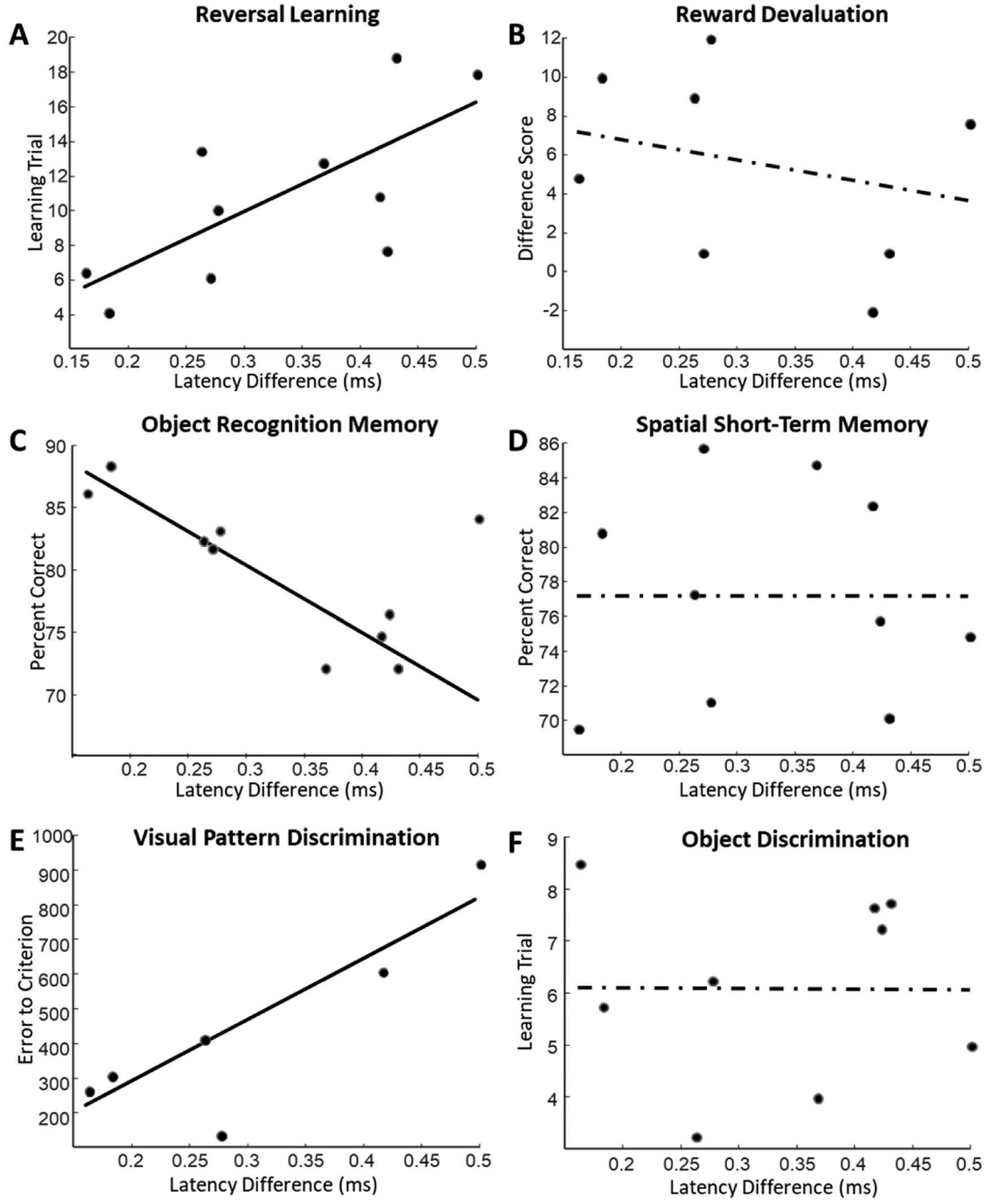

Figure 2. Task-specific relationships between auditory processing and cognition. (*A*) Scatter plot of auditory processing measures (temporal ABR latency differences) and the learning trials from the reversal learning task. (*B*) Scatter plot of auditory processing estimates and the difference score from the reward devaluation task. (*C*) Scatter plot of auditory processing estimates and performance on the object recognition task. (*D*) Scatter plot of auditory processing estimates and performance on the spatial short-term memory task. (*E*) Scatter plot of auditory processing estimates and performance on the visual discrimination of objects with overlapping features task. (*F*) Scatter plot of auditory processing estimates and the estimated learning trial on the object discrimination task.

$r = -0.64$, $t = -5.52$; Fig. 2C), and the temporal lobe-dependent visual discrimination of objects with overlapping features (robust regression; $n = 6$; $P = 0.032$, $r = 0.87$, $t = 3.23$; Fig. 2E). Conversely, estimates of auditory processing were not significantly associated with performance on the tests of reward devaluation (robust regression; $n = 8$; $P = 0.24$, $r = -0.49$, $t = -1.30$; Fig. 2B), spatial short-term memory (robust regression; $n = 10$; $P = 0.99$, $r = 0.0089$, $t = -0.0021$; Fig. 2D), or object discrimination (robust regression; $n = 9$; $P = 0.98$, $r = -0.017$, $t = -0.02$; Fig. 2F). These results indicate that relationships between auditory processing and cognition are cognitive domain-specific, rather than generalizable across distinct cognitive operations.

Importantly, age alone was not able to account for the observed covariations between sensory processing and cognition as tested by a statistical model incorporating age, sensory, and cognitive outcome measures (ANOVA; age $F(1,10) = 0.46$, $P = 0.51$). Rather there was a significant interaction between age, sensory and cognitive outcome measures (ANOVA; Age*Modality $F(1,10) = 22.76$, $P = 0.0023$).

Medial Temporal Lobe-Associated White Matter Integrity Is Associated with Auditory and Mnemonic Function

Diffusion MRI tractography approaches were used to assess the microstructural condition of white matter associated with the medial temporal lobe and frontal cortex. Two distinct approaches were used to account for the possibility that partial volume effects could have impacted FA estimates. Both approaches resulted in FA measures that were comparable and associated with auditory and cognitive function. The results from the more conservative approach are shown in the main text (Figs 3 and 4) and results from the other can be found in Supplementary Figs S7 and S8. In all cases normalized FA measures were extracted and relationships between these structural measures and cognitive and sensory functioning were assessed. Note that while it is not completely agreed upon what FA change reflects functionally, this scalar value has been used clinically to assess the microstructural condition of white matter tracts in both normal and pathological conditions (Mori and van Zijl 2002; Totenhagen et al. 2012), and is hypothesized to be an indication of white matter integrity.

Right hemisphere fimbria-fornix FA (Fig. 3A,B) was significantly lower in the aged macaques compared to adults (*t*-test, $P = 0.012$, $t = 3.16$; Fig. 3C), although there were no age or hemispheric differences when the left and right fimbria-fornix were analyzed together ($n_{adult} = 6$, $n_{aged} = 5$; ANOVA; age: $F(1,10) = 1.29$, $P = 0.27$; hem: $F(1,10) = 3.27$, $P = 0.09$). Intriguingly, the animals with greater right hemisphere fimbria-fornix FA also had better auditory processing scores (robust regression; $n = 10$; $P = 0.025$, $r = -0.74$, $t = -2.74$; Fig. 3D) and lower auditory pure-tone average thresholds (robust regression; $n = 10$; $P = 0.035$, $r = -0.71$, $t = -2.54$; Fig. 3E). Monkeys with higher right hemisphere fimbria-fornix FA also performed a temporal lobe-dependent visual discrimination task better than did animals with lower FA (robust regression, $n = 7$; $P = 0.04$, $r = -0.81$; $t = -2.73$; Fig. 3F). Left hemisphere fimbria-fornix FA was not associated with any measure of auditory or cognitive function (robust regression; VD: $n = 7$, $P = 0.70$, $r = 0.18$, $t = 0.41$; temporal ABR: $n = 10$; $P = 0.74$, $r = 0.13$, $t = 0.35$; threshold ABR: $n = 10$; $P = 0.81$, $r = 0.11$, $t = 0.24$), and FA measures from neither hemisphere were associated with visual system function (robust regression; $n = 10$; left hem $P = 0.77$, $r = -0.13$, $t = -0.30$; right hem: $P = 0.11$, $r = -0.48$, $t = -1.98$). Hippocampal commissure FA (Fig. 3G,H) was significantly lower in the aged macaques compared to adults ($n_{adult} = 6$, $n_{aged} = 5$; *t*-test, $P = 0.049$, $t = 2.28$; Fig. 3I). Similar to the case of the fimbria-fornix, monkeys with the highest hippocampal commissure FA exhibited trends indicating better auditory processing abilities ($n = 10$; robust regression, $r = -0.59$, $P = 0.09$); Fig. 3J) and lower auditory pure-tone average thresholds ($n = 10$; robust regression, $r = -0.62$, $P = 0.073$; Fig. 3K). Greater hippocampal commissure FA was, however, statistically significantly associated with better discrimination abilities (robust regression, $n = 7$; $P = 0.048$, $r = -0.78$; $t = -2.60$; Fig. 3L). Also like the fimbria-fornix, hippocampal commissure FA was not associated with visual system function (robust regression; $n = 10$; $P = 0.75$; $r = -0.12$; $t = -0.33$). Together these findings indicate that the structural variations reflected by FA estimates in hippocampus-associated white matter map onto individual differences in auditory and mnemonic function.

Frontal Cortex-Associated White Matter Connectivity Is not Associated with Auditory Processing

To test the anatomical specificity of the associations between hippocampus-associated white matter FA and auditory function, FA measures from two distinct frontal cortex-associated white matter tracts were extracted. Frontal thalamic radiation (Fig. 4A,B) FA was not different between adult and aged animals, nor was there a difference between the two hemispheres ($n_{adult} = 6$, $n_{aged} = 5$; ANOVA, age: $F(1,10) = 0.76$, $P = 0.40$; hem: $F(1,10) = 0.01$, $P = 0.99$; Fig. 4C). The FA of the frontal thalamic radiations was not associated with auditory processing (robust regression; $n = 10$; left hem $P = 0.63$, $r = -0.16$, $t = -0.49$; right hem: $P = 0.98$, $r = 0.005$, $t = 0.014$; Fig. 4D), nor with auditory pure-tone average thresholds (robust regression; $n = 10$; left hem: $P = 0.98$, $r = 0.03$, $t = 0.019$; right hem: $P = 0.52$, $r = 0.26$, $t = 0.68$; Fig. 4E). Similarly, the FA of the anterior commissure (Figs 4F,G) was not different between adult and aged animals ($n_{adult} = 6$, $n_{aged} = 5$; *t*-test, $P = 0.49$; $t = 0.73$; Fig. 4H), nor was it associated with auditory processing abilities ($n = 10$; robust regression, $P = 0.30$; $r = 0.40$, $t = 1.10$; Fig. 4I) or auditory pure-tone average thresholds ($n = 10$; robust regression, $P = 0.75$, $r = -0.15$, $t = -0.33$; Fig. 4J). Neither frontal thalamic radiation nor anterior commissure FA estimates were associated with VEP P_{75} latency differences (robust regression; $n = 10$; frontal radiation—left hem: $P = 0.88$; $r = 0.06$; $t = 0.15$; right hem: $P = 0.79$; $r = 0.10$; $t = 0.21$; anterior commissure: $P = 0.33$; $r = -0.38$; $t = -1.03$; data not shown).

Again, age alone was not able to account for the observed covariations between white matter FA, sensory outcome measures, and cognition (ANOVA; age $F = 1.36$, $P = 0.25$), and there was a significant interaction between age, FA, and sensory and cognitive processing scores (ANOVA; Age*FA*Modality $F = 9.45$, $P = 0.0007$). Together, these results indicate that the significant associations between medial temporal lobe-associated white matter FA and auditory temporal processing and visual discrimination abilities are not a result of general changes in white matter across the aging brain, and support the hypothesis that the temporal lobe may be particularly sensitive to functional and structural changes that cause auditory function and medial temporal lobe-dependent aspects of cognition to become associated in older animals (see Discussion).

Discussion

Several findings from this study support the conclusion that auditory processing abilities are selectively associated with medial temporal lobe-dependent mnemonic function in aging macaques. First, monkeys with better auditory processing showed superior performance on tasks known to require the integrity of medial temporal lobe brain structures. In contrast, behaviors examined that require frontal cortical networks for task solution were not associated with differential levels of auditory processing. Second, a similar pattern of results was observed between the FA, as assessed by dMRI, of subcortical- and interhemispheric-projecting hippocampal white matter tracts and behavior. Specifically, higher FA of hippocampal white matter was related to better performance on tasks dependent

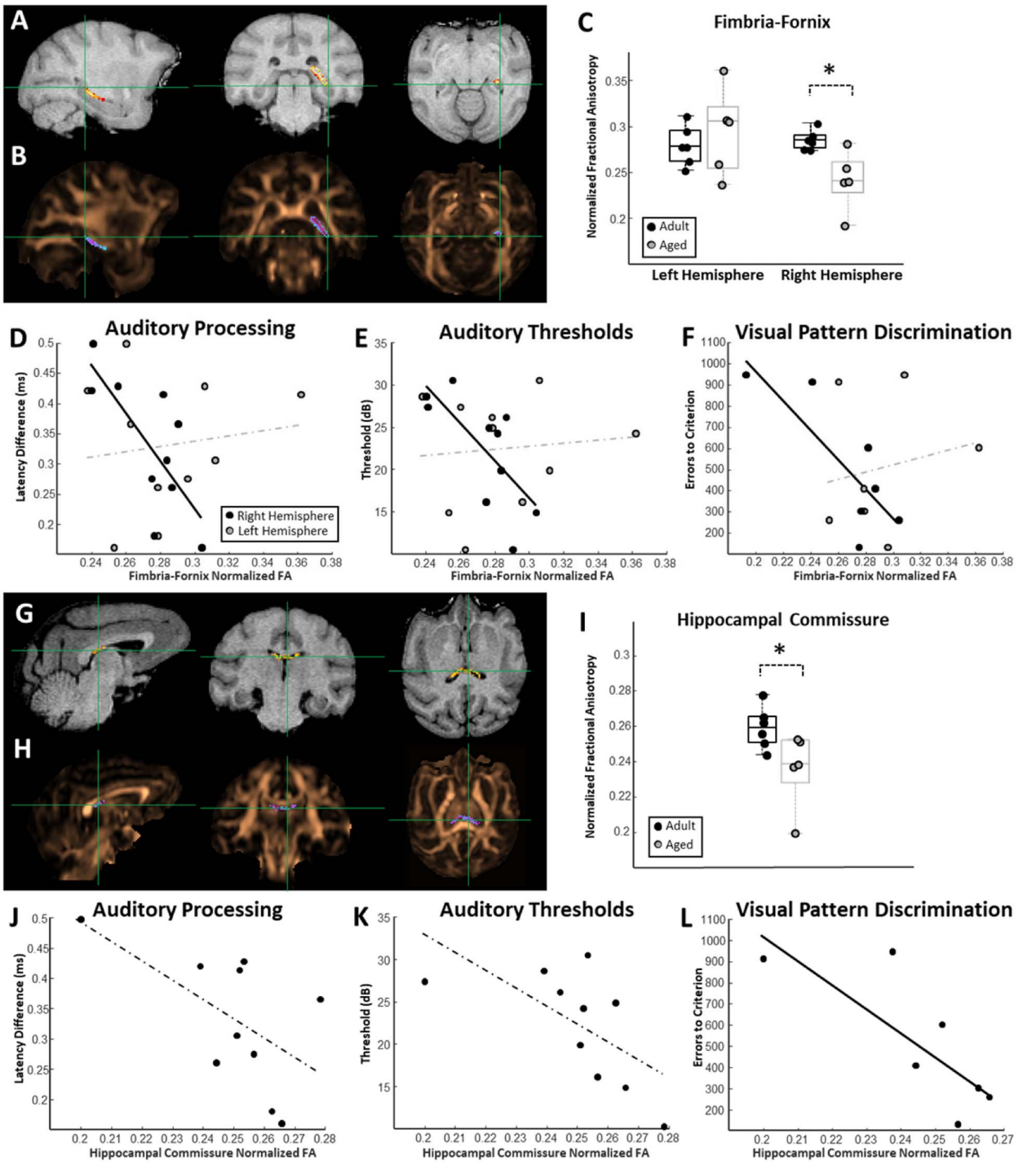

Figure 3. Relationships between hippocampus-associated white matter connectivity and auditory and mnemonic function. (*A*) Representative probability map of voxels belonging to the right hemisphere fimbria-fornix overlaid on a T1-weighted MRI. (*B*) The same probability map overlaid on a FA map pseudocolored in copper. (*C*) Box and whisker plots of fimbria-fornix FA estimates for each individual monkey separated by left and right hemisphere. Boxes represent the middle 50% of the data, and horizontal lines mark the median of each distribution. Each filled circle indicates an individual monkey, with black circles representing adult animals and gray representing the aged. Right hemisphere fimbria-fornix FA was significantly lower in aged macaques compared to adults. (*D*) Relationship between fimbria-fornix FA estimates and estimates of auditory processing (temporal ABR). A significant relationship was observed between right hemisphere fimbria-fornix FA and auditory processing capacities. (*E*) Relationship between fimbria-fornix FA and auditory pure-tone average thresholds. A significant relationship was observed between right hemisphere fimbria-fornix FA and auditory thresholds. (*F*) Relationship between fimbria-fornix FA and the number of errors to criterion on the visual discrimination task. A significant association was observed between right hemisphere fimbria-fornix FA and visual discrimination performance. Left hemisphere fimbria-fornix connectivity was not associated with visual discrimination, auditory processing, or auditory thresholds. (*G*) Representative probability map of voxels belonging to the hippocampal commissure overlaid on a T1-weighted MRI. (*H*) The same probability map overlaid on a FA map pseudocolored in copper. (*I*) Box and whisker plot of hippocampal commissure FA estimates for each individual monkey. Aged monkeys had significantly lower hippocampal commissure FA than adults. Box and whisker plot as in (*C*). (*J*) Relationship between hippocampal commissure FA estimates and estimates of auditory processing. (*K*) Relationship between hippocampal commissure FA and auditory pure-tone thresholds. (*L*) Relationship between hippocampal commissure FA and the number of errors to criterion on the visual discrimination task. A significant relationship was observed between hippocampal commissure FA and visual discrimination abilities.

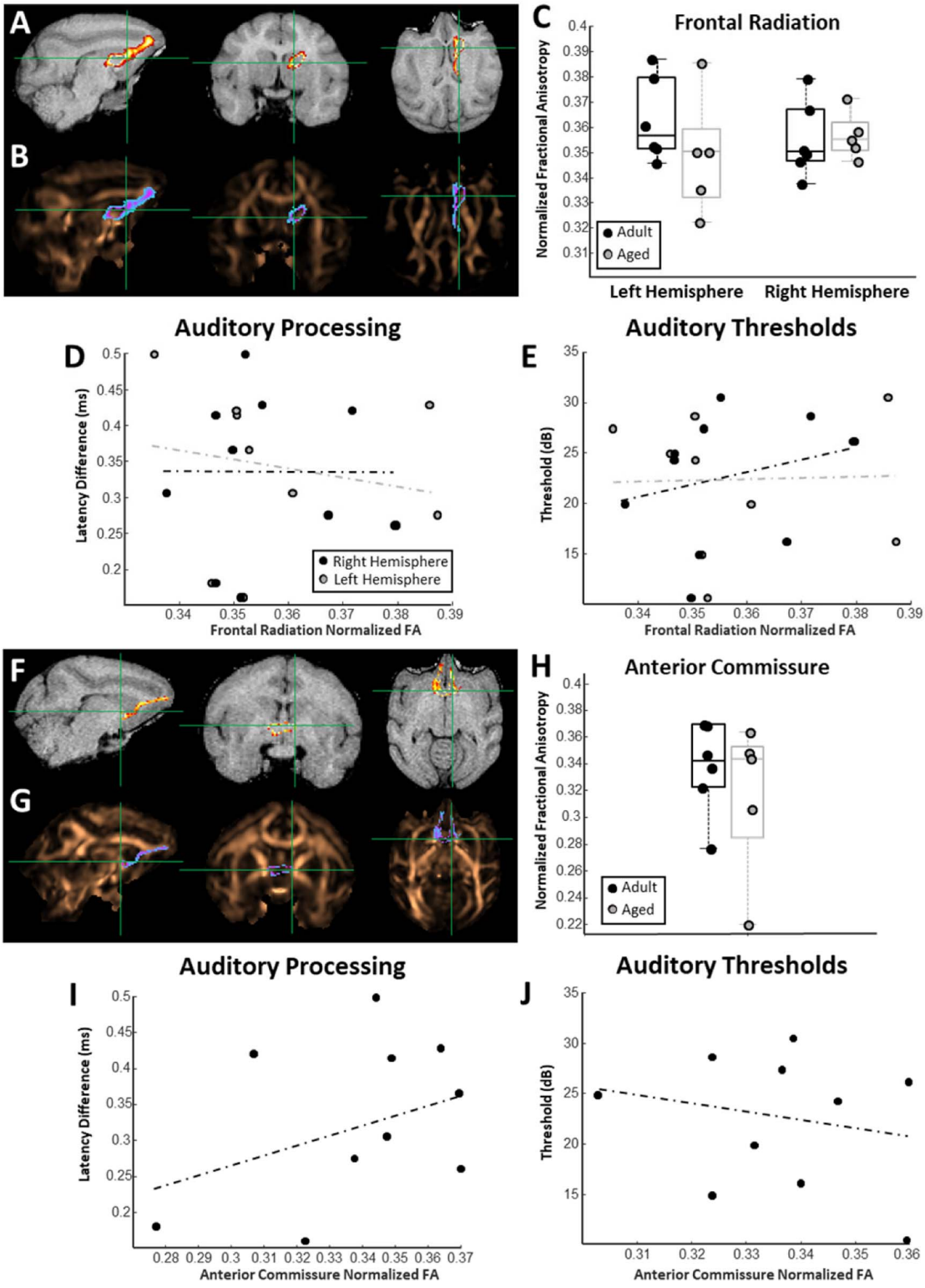

Figure 4. Relationships between frontal cortex-associated white matter connectivity and auditory function. (*A*) Representative probability map of voxels belonging to the right hemisphere frontal thalamic radiation overlaid on a T1-weighted MRI. (*B*) The same probability map overlaid on a FA map pseudocolored in copper. (*C*) Box and whisker plots of frontal thalamic radiation FA estimates for each individual monkey separated by left and right hemisphere. Boxes represent the middle 50% of the data, and horizontal lines mark the median of each distribution. Each filled circle indicates an individual monkey, with black circles representing adult animals and gray representing the aged. (*D*) Relationship between frontal thalamic radiation FA and estimates of auditory processing. In all scatterplots solid trend line indicate statistically significant relationships, and dotted trend lines represent nonsignificant relationships. (*E*) Relationship between frontal thalamic radiation FA estimates and auditory pure-tone average thresholds. (*F*) Representative probability map of voxels belonging to the anterior commissure overlaid on a T1-weighted MRI. (*G*) The same probability map overlaid on a FA map pseudocolored in copper. (*H*) Box and whisker plots of anterior commissure FA estimates for each individual monkey. Box and whisker plot as in (*C*). (*I*) Relationship between anterior commissure FA and estimates of auditory processing. (*J*) Relationship between anterior commissure FA estimates and auditory pure-tone average thresholds.

on medial temporal lobe structures, but not tasks dependent on frontal lobe structures. Finally, higher auditory processing abilities and lower acoustic thresholds were associated with higher FA in long-range white matter tracts connecting the hippocampus to other cortical and subcortical regions. There was no relationship between FA in frontal cortical white matter tracts and auditory function. Moreover, visual sensory function measures were not associated with any of the behaviors examined, or the FA of any white matter tract assessed.

Auditory Processing Is Associated with Medial Temporal Lobe-Dependent Cognition

In this study, multiple estimates of cognitive and sensory function were acquired within the same group of monkeys ranging in age from young adult to old. This allowed an assessment of whether the cognitive or sensory measures changed in tandem or showed unique patterns of change across age. Although auditory thresholds were not associated with any aspect of cognition in these animals, superior auditory temporal processing was related to better overall cognitive function as assessed by a composite score of the six tasks contained within the behavioral battery. Three particular cognitive functions drove the association between better auditory processing and higher overall cognition–concurrent reversal learning, object recognition memory, and visual discriminations of stimuli with overlapping features (Fig. 2). Reward devaluation, spatial short-term memory, and object discrimination abilities, on the other hand, showed no relationship with auditory processing in these animals. Together these observations indicate that auditory processing abilities functionally covary with specific aspects of cognition in aging macaques regardless of auditory acuity.

The three tasks that were related to auditory processing are known from previous lesion studies in macaques to depend on the integrity of brain structures in the medial temporal lobe. For the concurrent reversal learning task, it is known that lesions to the inferotemporal cortex result in impairments (Wilson and Gaffan 2008). The object recognition memory and visual discrimination tasks, on the other hand, are known to require interactions between the adjacent perirhinal cortex and other medial temporal lobe structures (Zola-Morgan et al. 1989; Buffalo et al. 2000; Baxter and Murray 2001; Yassa and Stark 2011). Two cognitive functions not associated with auditory processing, reward devaluation and spatial short-term memory, have a stronger reliance on orbitofrontal and dorsolateral prefrontal cortex integrity, respectively (Funahashi et al. 1993; Baxter et al. 2000; Rudebeck et al. 2013). The FA of the frontal thalamic radiation and the anterior commissure that connects prefrontal cortical structures with other brain areas was not associated with these two behaviors in our study. This could suggest either that different frontal cortical white matter systems are more important in these behaviors, or that these particular behaviors are independent of frontal cortex white matter condition.

One thing to consider in interpreting these data is that the bulk of auditory processing in the macaque forebrain occurs in the temporal lobe, primarily along the superior temporal gyrus (Kaas and Hackett 2000; Recanzone and Sutter 2008). Thus, some of the specificity in these relationships might be explained by heterogeneity in patterns of molecular and cellular aging between the frontal and temporal lobes. This could bias brain functions with neuroanatomical substrates within the same lobe to functionally covary across the lifespan more than brain functions driven by more anatomically segregated circuits.

Auditory Processing Is Associated with Hippocampus White Matter FA and Cognitive Performance in Specific Domains

Diffusion MRI results were also analyzed to determine whether sensory and cognitive processing abilities are associated with the FA of circuits in the medial temporal lobe and frontal cortex. Monkeys with higher FA values in the hippocampal commissure and right hemisphere fimbria-fornix showed a better ability to discriminate stimuli with overlapping features in a temporal lobe-dependent visual discrimination task. This agrees with the current understanding that neuronal computations in medial temporal lobe networks give rise to this cognitive function (Baxter and Murray 2001; Bartko et al. 2007; Yassa and Stark 2011; Ahn and Lee 2015). Animals with higher FA in both pathways also had greater auditory processing abilities and lower acoustic thresholds. These data indicate that age-associated structural and functional alterations in the medial temporal lobe that worsen the ability to discriminate visual patterns with high feature overlap occur alongside the structural and functional changes that reduce auditory processing in older individuals. These dMRI data might provide a functional explanation for the observation that animals with better visual discrimination abilities had superior auditory processing (Fig. 2).

Auditory processing abilities and pure-tone average thresholds were not associated with FA in two distinct frontal cortex-associated projection systems (Fig. 4). This indicates that the observed relationships between auditory processing and hippocampus-associated white matter FA is not due to global changes in white-matter composition across the aging brain. Together these results further suggest that auditory temporal processing and medial temporal lobe-dependent cognitive function become associated across the lifespan in part due to differential alterations in temporal versus frontal lobe function.

Visual Processing Ability Was not Correlated with Auditory Processing, White Matter Tract Integrity, or Cognition

Given the strong associations observed between audition, white matter FA, and cognition, it was surprising that visual responses did not show any association with the measurements of brain and cognitive function tested here. Because we did not conduct exhaustive cognitive and sensory tests, we cannot rule out that associations may emerge if dMRI analyses of other white matter tracts and behaviors are carried out in future experiments.

Potential Factors Driving Regionally Selective Functional Covariations across the Lifespan

A number of factors might be responsible for the associations observed between specific brain regions, sensory and cognitive function during the aging process. Among others, sharing vascular perfusion characteristics, specific intralobular connectivity patterns, or lobe-specific embryological origins might be considered.

It is possible that regional differences in neurovascular function between the frontal and temporal lobes may bias auditory abilities to covary with medial temporal lobe-dependent cognitive operations. Neurovascular dysfunction is often observed during normative aging and can initiate a series of molecular events that influence physiology in the regions impacted (Nelson et al. 2016; Sweeney et al. 2018). There is evidence that

occlusions of specific cerebral arteries give rise to task-specific cognitive impairments (Fabiani et al. 2014), indicating that not all brain functions are impacted equally following a given vascular insult. Thus, it is not unreasonable to propose that lobar differences in neurovascular function across the lifespan could contribute to the covariation between temporal lobe sensory and cognitive operations. This hypothesis is potentially experimentally testable and could be accomplished by combining regional measures of vascular function with tests of sensory and cognitive tests dependent on networks within specific brain areas.

Another possibility is that the extent of neuronal connectivity between regions determines the degree to which their functions covary, possibly through side effects associated with age-associated hyperexcitability (Juarez-Salinas et al. 2010; Yassa et al. 2011; Thomé et al. 2015) or changes in synaptic function (Burke and Barnes 2006; Hara et al. 2012; Morrison and Baxter 2012). In support of this idea, anatomical tract-tracing studies indicate that auditory cortex sends direct projections to and receives projections from brain regions in the medial temporal lobe, including the perirhinal and parahippocampal cortices (Seltzer and Pandya 1978; Suzuki and Amaral 1994; Kaas and Hackett 1998). A connectivity hypothesis of functional covariation of sensory and cognitive operations can only partially explain these observations, however, because long-range connections also exist between the auditory cortices and the frontal lobe (Romanski et al. 1999).

Finally, distinct embryological origins and developmental trajectories of the frontal and temporal lobes may predispose cells and circuits in each lobe to succumb to different age-related risk factors. For example, inhibitory interneurons that migrate into frontal and parietal cortices have a distinctly different pattern of transcription factor expression (i.e., enriched with COUP-TFII and Sp8) from those destined to migrate into temporal and occipital cortices (that are enriched with Sox6) (Ma et al. 2013). It possible that inhibitory cells in the temporal lobe, known to participate in circuit excitability with aging, are differentially vulnerable to the effects of age. This hypothesis is consistent with the idea that frontal cortical interneurons are somehow protected against these age-related changes because of different patterns of gene expression. In support of this is the observation from single unit recording studies conducted in rhesus macaques that firing rates are not elevated with age in frontal lobe networks (Wang et al. 2011), suggesting preservation of excitatory/inhibitory circuit balance in this region.

These hypotheses are not necessarily mutually exclusive, and remain to be verified by empirical examination. Wingfield and colleagues have suggested that auditory processing deficits impact cognition through supplementary recruitments of certain frontal and temporoparietal brain regions during acoustic information processing in older individuals (Peelle et al. 2010; Peelle et al. 2011). The data presented in this study suggest that one factor contributing to the differential use of circuits required for normal acoustic performance in older people may be the vulnerability of the temporal lobe during aging. This may trigger a recruitment of circuits that can compensate for and normalize behaviors that would otherwise be impaired in older individuals.

Conclusion

The present study combined electrophysiological assessments of auditory and visual system function with dMRI in a colony of behaviorally characterized aging macaques. The results indicate that auditory system function, temporal lobe-dependent cognition and white-matter composition covary across age. This relationship to auditory function was not observed with frontal lobe-dependent tasks or frontal lobe white matter characteristics. This suggests that sensory and cognitive functions driven by temporal lobe processing are impacted by age in a selective manner in part due to regionally selective structural and functional variations. Future studies designed to understand covariations in the impact of aging on distinct sensory and cognitive brain regions will further our understanding of how neuronal networks compensate for, and adapt to functional alterations that arise across the aging brain. Such studies will not only provide fruitful insights into sensory contributions to cognitive decline in older humans, but also may illuminate better approaches to reduce the incidence of cognitive impairments that arise from normative brain aging and neurodegenerative disease.

Supplementary Material

Supplementary material is available at *Cerebral Cortex* online.

Funding

National Institutes of Health (grants RO1 AG050548, F31 AG055263); the McKnight Brain Research Foundation; and State of Arizona, DHS.

Notes

We are grateful to Mike Valdez for design and fabrication of the MRI-compatible nonhuman primate stereotactic frame, Scott Squire for assistance in MRI, Kojo Plange for behavioral training, and Luann Snyder and Michelle Albert for administrative assistance. *Conflict of Interest*: None declared.

References

Ahn J-R, Lee I. 2015. Neural correlates of object-associated choice behavior in the perirhinal cortex of rats. *J Neurosci*. 35(4):1692–1705. doi: 10.1523/JNEUROSCI.3160-14.2015.

Allen AR, Starr A. 1978. Auditory brain stem potentials in monkey (M. mulatta) and man. *Electroencephalogr Clin Neurophysiol*. 45(1):53–63.

Andersson JLR, Sotiropoulos SN. 2015. Non-parametric representation and prediction of single- and multi-shell diffusion-weighted MRI data using Gaussian processes. *NeuroImage*. 122(Supplement C):166–176. doi: 10.1016/j.neuroimage.2015.07.067.

Bakker R, Tiesinga P, Kötter R. 2015. The scalable brain Atlas: instant web-based access to public brain atlases and related content. *Neuroinformatics*. 13(3):353–366. doi: 10.1007/s12021-014-9258-x.

Bartko SJ, Winters BD, Cowell RA, Saksida LM, Bussey TJ. 2007. Perceptual functions of perirhinal cortex in rats: zero-delay object recognition and simultaneous oddity discriminations. *J Neurosci Off J Soc Neurosci*. 27(10):2548–2559. doi: 10.1523/JNEUROSCI.5171-06.2007.

Baxter MG, Murray EA. 2001. Impairments in visual discrimination learning and recognition memory produced by neurotoxic lesions of rhinal cortex in rhesus monkeys. *Eur J Neurosci*. 13(6):1228–1238.

Baxter MG, Parker A, Lindner CCC, Izquierdo AD, Murray EA. 2000. Control of response selection by Reinforcer value requires interaction of amygdala and orbital prefrontal cortex. *J Neurosci*. 20(11):4311–4319.

Buffalo EA, Ramus SJ, Squire LR, Zola SM. 2000. Perception and recognition memory in monkeys following lesions of area TE and perirhinal cortex. *Learn Mem Cold Spring Harb N*. 7(6):375–382.

Burke SN, Barnes CA. 2006. Neural plasticity in the ageing brain. *Nat Rev Neurosci*. 7(1):30–40. doi: 10.1038/nrn1809.

Burke SN, Thome A, Plange K, Engle JR, Trouard TP, Gothard KM, Barnes CA. 2014. Orbitofrontal cortex volume in area 11/13 predicts reward devaluation, but not reversal learning performance, in young and aged monkeys. *J Neurosci*. 34(30):9905–9916. doi: 10.1523/JNEUROSCI.3918-13.2014.

Burke SN, Wallace JL, Hartzell AL, Nematollahi S, Plange K, Barnes CA. 2011. Age-associated deficits in pattern separation functions of the Perirhinal cortex: a cross-species consensus. *Behav Neurosci*. 125(6):836–847. doi: 10.1037/a0026238.

Comrie AE, Gray DT, Smith AC, Barnes CA. 2018. Different macaque models of cognitive aging exhibit task-dependent behavioral disparities. *Behav Brain Res*. 344:110–119. doi: 10.1016/j.bbr.2018.02.008.

Deal JA, Betz J, Yaffe K, Harris T, Purchase-Helzner E, Satterfield S, Pratt S, Govil N, Simonsick EM, Lin FR. 2017. Hearing impairment and incident dementia and cognitive decline in older adults: the health ABC study. *J Gerontol A Biol Sci Med Sci*. 72(5):703–709. doi: 10.1093/gerona/glw069.

Eggermont JJ. 2015. Animal models of auditory temporal processing. *Int J Psychophysiol*. 95(2):202–215. doi: 10.1016/j.ijpsycho.2014.03.011.

Engle JR, Tinling S, Recanzone GH. 2013. Age-related hearing loss in rhesus monkeys is correlated with Cochlear Histopathologies. *PLOS ONE*. 8(2):e55092. doi: 10.1371/journal.pone.0055092.

Fabiani M, Low KA, Tan C-H, Zimmerman B, Fletcher MA, Schneider-Garces N, Maclin EL, Chiarelli AM, Sutton BP, Gratton G. 2014. Taking the pulse of aging: mapping pulse pressure and elasticity in cerebral arteries with optical methods. *Psychophysiology*. 51(11):1072–1088. doi: 10.1111/psyp.12288.

Fernandes MA, Davidson PSR, Glisky EL, Moscovitch M. 2004. Contribution of frontal and temporal lobe function to memory interference from divided attention at retrieval. *Neuropsychology*. 18(3):514–525. doi: 10.1037/0894-4105.18.3.514.

Fowler CG, Chiasson KB, Leslie TH, Thomas D, Beasley TM, Kemnitz JW, Weindruch R. 2010. Auditory function in rhesus monkeys: effects of aging and caloric restriction in the Wisconsin monkeys five years later. *Hear Res*. 261(1–2):75–81. doi: 10.1016/j.heares.2010.01.006.

Funahashi S, Bruce CJ, Goldman-Rakic PS. 1993. Dorsolateral prefrontal lesions and oculomotor delayed-response performance: evidence for mnemonic "scotomas". *J Neurosci*. 13(4):1479–1497.

Glisky EL, Polster MR, Routhieaux BC. 1995. Double dissociation between item and source memory. *Neuropsychology*. 9(2):229–235. doi: 10.1037/0894-4105.9.2.229.

Gopinath B, Rochtchina E, Wang JJ, Schneider J, Leeder SR, Mitchell P. 2009. Prevalence of age-related hearing loss in older adults: blue Mountains study. *Arch Intern Med*. 169(4):415–418. doi: 10.1001/archinternmed.2008.597.

Gray DT, Recanzone GH. 2017. 3.19 - Individual Variability in the Functional Organization of the Cerebral Cortex Across a Lifetime: A Substrate for Evolution Across Generations A2 - Kaas, Jon H. In: *Evolution of Nervous Systems* (Second Edition). Oxford: Academic Press. p. 343–356. http://www.sciencedirect.com/science/article/pii/B978012804042300097X (last accessed 13 January 2017).

Gray DT, Smith AC, Burke SN, Gazzaley A, Barnes CA. 2017. Attentional updating and monitoring and affective shifting are impacted independently by aging in macaque monkeys. *Behav Brain Res*. 322(Part B):329–338. doi: 10.1016/j.bbr.2016.06.056.

Gray DT, Umapathy L, Burke SN, Trouard TP, Barnes CA. 2018. Tract-specific white matter correlates of age-related reward devaluation deficits in macaque monkeys. *J Neuroimaging Psychiatry Neurol*. 3(2):13–26. doi: 10.17756/jnpn.2018-023.

Greve DN, Fischl B. 2009. Accurate and robust brain image alignment using boundary-based registration. *NeuroImage*. 48(1):63–72. doi: 10.1016/j.neuroimage.2009.06.060.

Hara Y, Rapp PR, Morrison JH. 2012. Neuronal and morphological bases of cognitive decline in aged rhesus monkeys. *Age*. 34(5):1051–1073. doi: 10.1007/s11357-011-9278-5.

Harlow HF, Bromer JA. 1938. A test apparatus for monkeys. *Psychol Rec*. 2:433–435.

Humes LE, Busey TA, Craig J, Kewley-Port D. 2013. Are age-related changes in cognitive function driven by age-related changes in sensory processing? *Atten Percept Psychophys*. 75(3):508–524. doi: 10.3758/s13414-012-0406-9.

Jayakody DMP, Almeida OP, Speelman CP, Bennett RJ, Moyle TC, Yiannos JM, Friedland PL. 2018. Association between speech and high-frequency hearing loss and depression, anxiety and stress in older adults. *Maturitas*. 110:86–91. doi: 10.1016/j.maturitas.2018.02.002.

Jayakody DMP, Friedland PL, Nel E, Martins RN, Atlas MD, Sohrabi HR. 2017. Impact of Cochlear implantation on cognitive functions of older adults: pilot test results. *Otol Neurotol*. 38(8):e289–e295. doi: 10.1097/MAO.0000000000001502.

Juarez-Salinas DL, Engle JR, Navarro XO, Recanzone GH. 2010. Hierarchical and serial processing in the spatial auditory cortical pathway is degraded by natural aging. *J Neurosci*. 30(44):14795–14804. doi: 10.1523/JNEUROSCI.3393-10.2010.

Kaas JH, Hackett TA. 1998. Subdivisions of auditory cortex and levels of processing in primates. *Audiol Neurootol*. 3(2–3):73–85. doi: 10.1159/000013783.

Kaas JH, Hackett TA. 2000. Subdivisions of auditory cortex and processing streams in primates. *Proc Natl Acad Sci*. 97(22):11793–11799. doi: 10.1073/pnas.97.22.11793.

Kiebzak GM. 1991. Age-related bone changes. *Exp Gerontol*. 26(2–3):171–187.

Lehman JF, Greenberg BD, McIntyre CC, Rasmussen SA, Haber SN. 2011. Rules ventral prefrontal cortical axons use to reach their targets: implications for diffusion tensor imaging tractography and deep brain stimulation for psychiatric illness. *J Neurosci*. 31(28):10392–10402. doi: 10.1523/JNEUROSCI.0595-11.2011.

Lin FR. 2011. Hearing loss and cognition among older adults in the United States. *J Gerontol Ser A*. 66A(10):1131–1136. doi: 10.1093/gerona/glr115.

Ma T, Wang C, Wang L, Zhou X, Tian M, Zhang Q, Zhang Y, Li J, Liu Z, Cai Y *et al*. 2013. Subcortical origins of human and monkey neocortical interneurons. *Nat Neurosci*. 16(11):1588–1597. doi: 10.1038/nn.3536.

Manjón JV, Coupé P, Concha L, Buades A, Collins DL, Robles M. 2013. Diffusion weighted image denoising using overcomplete local PCA. *PLOS ONE*. 8(9):e73021. doi: 10.1371/journal.pone.0073021.

Mehraei G, Gallardo AP, Shinn-Cunningham BG, Dau T. 2017. Auditory brainstem response latency in forward masking, a marker of sensory deficits in listeners with normal hearing thresholds. *Hear Res*. 346:34–44. doi: 10.1016/j.heares.2017.01.016.

Mehraei G, Hickox AE, Bharadwaj HM, Goldberg H, Verhulst S, Liberman MC, Shinn-Cunningham BG. 2016. Auditory brainstem response latency in noise as a marker of cochlear synaptopathy. *J Neurosci*. 36(13):3755–3764. doi: 10.1523/JNEUROSCI.4460-15.2016.

Mick P, Kawachi I, Lin FR. 2014. The association between hearing loss and social isolation in older adults. *Otolaryngol Head Neck Surg*. 150(3):378–384. doi: 10.1177/0194599813518021.

Moore TL, Killiany RJ, Herndon JG, Rosene DL, Moss MB. 2006. Executive system dysfunction occurs as early as middle-age in the rhesus monkey. *Neurobiol Aging*. 27(10):1484–1493. doi: 10.1016/j.neurobiolaging.2005.08.004.

Mori S, van Zijl PCM. 2002. Fiber tracking: principles and strategies - a technical review. *NMR Biomed*. 15(7–8):468–480. doi: 10.1002/nbm.781.

Morrison JH, Baxter MG. 2012. The ageing cortical synapse: hallmarks and implications for cognitive decline. *Nat Rev Neurosci*. 13(4):240–250. doi: 10.1038/nrn3200.

Mosekilde L. 2000. Age-related changes in bone mass, structure, and strength–effects of loading. *Z Rheumatol*. 59(Suppl 1):1–9.

Nelson AR, Sweeney MD, Sagare AP, Zlokovic BV. 2016. Neurovascular dysfunction and neurodegeneration in dementia and Alzheimer's disease. *Biochim Biophys Acta*. 1862(5):887–900. doi: 10.1016/j.bbadis.2015.12.016.

Ng C-W, Navarro X, Engle JR, Recanzone GH. 2015. Age-related changes of auditory brainstem responses in nonhuman primates. *J Neurophysiol*. 114(1):455–467. doi: 10.1152/jn.00663.2014.

Panza F, Solfrizzi V, Seripa D, Imbimbo BP, Capozzo R, Quaranta N, Pilotto A, Logroscino G. 2015. Age-related hearing impairment and frailty in Alzheimer's disease: interconnected associations and mechanisms. *Front Aging Neurosci*. 7. doi: 10.3389/fnagi.2015.00113. https://www.ncbi.nlm.nih.gov/pmc/articles/PMC4460423/ last accessed 16 August 2018.

Peelle JE, Troiani V, Grossman M, Wingfield A. 2011. Hearing loss in older adults affects neural systems supporting speech comprehension. *J Neurosci*. 31(35):12638–12643. doi: 10.1523/JNEUROSCI.2559-11.2011.

Peelle JE, Troiani V, Wingfield A, Grossman M. 2010. Neural processing during older adults' comprehension of spoken sentences: age differences in resource allocation and connectivity. *Cereb Cortex*. 20(4):773–782. doi: 10.1093/cercor/bhp142.

Pierpaoli C, Walker L, Irfanoglu MO, Barnett A, Basser P, Chang LC, Koay C, Pajevic S, Rohde G, Sarlls J. 2010. TORTOISE: an integrated software package for processing of diffusion MRI data. In: *ISMRM 18th annual meeting*. Stockholm, Sweden: ISMRM, p. 1597.

Rasmussen CE, Williams CKI. 2006. *Gaussian processes for machine learning*. Cambridge, MA, USA: MIT Press. (last accessed 2 January 2018). http://publications.eng.cam.ac.uk/325766/.

Recanzone GH, Sutter ML. 2008. The biological basis of audition. *Annu Rev Psychol*. 59. doi: 10.1146/annurev.psych.59.103006.093544. https://www.ncbi.nlm.nih.gov/pmc/articles/PMC3856181/ last accessed 11 January 2018.

Romanski LM, Tian B, Fritz J, Mishkin M, Goldman-Rakic PS, Rauschecker JP. 1999. Dual streams of auditory afferents target multiple domains in the primate prefrontal cortex. *Nat Neurosci*. 2(12):1131–1136. doi: 10.1038/16056.

Rudebeck PH, Saunders RC, Prescott AT, Chau LS, Murray EA. 2013. Prefrontal mechanisms of behavioral flexibility, emotion regulation and value updating. *Nat Neurosci*. 16(8):1140–1145. doi: 10.1038/nn.3440.

Seltzer B, Pandya DN. 1978. Afferent cortical connections and architectonics of the superior temporal sulcus and surrounding cortex in the rhesus monkey. *Brain Res*. 149(1):1–24. doi: 10.1016/0006-8993(78)90584-X.

Smith AC, Frank LM, Wirth S, Yanike M, Hu D, Kubota Y, Graybiel AM, Suzuki WA, Brown EN. 2004. Dynamic analysis of learning in Behavioral experiments. *J Neurosci*. 24(2):447–461. doi: 10.1523/JNEUROSCI.2908-03.2004.

Suzuki WL, Amaral DG. 1994. Perirhinal and parahippocampal cortices of the macaque monkey: cortical afferents. *J Comp Neurol*. 350(4):497–533. doi: 10.1002/cne.903500402.

Sweeney MD, Kisler K, Montagne A, Toga AW, Zlokovic BV. 2018. The role of brain vasculature in neurodegenerative disorders. *Nat Neurosci*. 21(10):1318. doi: 10.1038/s41593-018-0234-x.

Thomé A, Gray DT, Erickson CA, Lipa P, Barnes CA. 2015. Memory impairment in aged primates is associated with region-specific network dysfunction. *Mol Psychiatry*. . doi: 10.1038/mp.2015.160. http://www.nature.com/mp/journal/vaop/ncurrent/full/mp2015160a.html last accessed 24 March 2016.

Totenhagen JW, Lope-Piedrafita S, Borbon IA, Yoshimaru ES, Erickson RP, Trouard TP. 2012. In vivo assessment of neurodegeneration in Niemann-pick type C mice by quantitative T2 mapping and diffusion tensor imaging. *J Magn Reson Imaging JMRI*. 35(3):528–536. doi: 10.1002/jmri.22837.

Tustison N, Gee J. 2009. N4ITK: Nick's N3 ITK implementation for MRI bias field correction. *Insight J*. .

Tustison NJ, Avants BB, Cook PA, Zheng Y, Egan A, Yushkevich PA, Gee JC. 2010. N4ITK: improved N3 bias correction. *IEEE Trans Med Imaging*. 29(6):1310–1320.

Wang M, Gamo NJ, Yang Y, Jin LE, Wang X-J, Laubach M, Mazer JA, Lee D, Arnsten AFT. 2011. Neuronal basis of age-related working memory decline. *Nature*. 476(7359):210–213. doi: 10.1038/nature10243.

Wattamwar K, Qian ZJ, Otter J, Leskowitz MJ, Caruana FF, Siedlecki B, Spitzer JB, Lalwani AK. 2017. Increases in the rate of age-related hearing loss in the older old. *JAMA Otolaryngol Neck Surg*. 143(1):41–45. doi: 10.1001/jamaoto.2016.2661.

Wilson CRE, Gaffan D. 2008. Prefrontal–inferotemporal interaction is not always necessary for reversal learning. *J Neurosci*. 28(21):5529–5538. doi: 10.1523/JNEUROSCI.0952-08.2008.

Yassa MA, Mattfeld AT, Stark SM, Stark CEL. 2011. Age-related memory deficits linked to circuit-specific disruptions in the hippocampus. *Proc Natl Acad Sci U S A*. 108(21):8873–8878. doi: 10.1073/pnas.1101567108.

Yassa MA, Stark CEL. 2011. Pattern separation in the hippocampus. *Trends Neurosci*. 34(10):515–525. doi: 10.1016/j.tins.2011.06.006.

Zola-Morgan S, Squire LR, Amaral DG, Suzuki WA. 1989. Lesions of perirhinal and parahippocampal cortex that spare the amygdala and hippocampal formation produce severe memory impairment. *J Neurosci*. 9(12):4355–4370. doi: 10.1523/JNEUROSCI.09-12-04355.1989.